Available online at www.sciencedirect.com
ScienceDirect
Icarus 195 (2008) 1–15
ICARUS
www.elsevier.com/locate/icarus

Global MHD modeling of Mercury's magnetosphere with applications to the MESSENGER mission and dynamo theory

K. Kabin [a,*], M.H. Heimpel [a], R. Rankin [a], J.M. Aurnou [b], N. Gómez-Pérez [a,1], J. Paral [a], T.I. Gombosi [c], T.H. Zurbuchen [c], P.L. Koehn [d], D.L. DeZeeuw [c]

[a] *Department of Physics, The University of Alberta, Edmonton, Alberta, T6G 2G7, Canada*
[b] *Department of Earth and Space Sciences, University of California, Los Angeles, CA 90095, USA*
[c] *Atmospheric, Oceanic and Space Science, University of Michigan, Ann Arbor, MI 48109, USA*
[d] *Eastern Michigan University, Department of Physics and Astronomy, Ypsilanti, MI 48197, USA*

Received 29 June 2007; revised 15 November 2007

Available online 8 January 2008

Abstract

We use a global magnetohydrodynamic (MHD) model to simulate Mercury's space environment for several solar wind and interplanetary magnetic field (IMF) conditions in anticipation of the magnetic field measurements by the MESSENGER spacecraft. The main goal of our study is to assess what characteristics of the internally generated field of Mercury can be inferred from the MESSENGER observations, and to what extent they will be able to constrain various models of Mercury's magnetic field generation. Based on the results of our simulations, we argue that it should be possible to infer not only the dipole component, but also the quadrupole and possibly even higher harmonics of the Mercury's planetary magnetic field. We furthermore expect that some of the crucial measurements for specifying the Hermean internal field will be acquired during the initial fly-bys of the planet, before MESSENGER goes into orbit around Mercury.

Keywords: Mercury, interiors; Magnetospheres

1. Introduction

The Hermean magnetosphere has been visited by only one spacecraft, Mariner 10, so far, but it is now targeted for investigation by the MESSENGER mission (Solomon et al., 2001; Gold et al., 2001), which is currently underway, as well as Bepi-Colombo (McNutt et al., 2004) to be launched in 2013. Before being inserted into orbit around Mercury in March 2011, the MESSENGER spacecraft is scheduled to perform three fly-bys of Mercury in 2008 and 2009 which should also provide very important new observations.

Mariner 10 data showed that Mercury has a weak magnetic field with a surface strength of roughly 300 nT—less than 1/100 the magnitude of Earth's surface field. Nevertheless, Mercury's field seems to be global and approximately dipolar, with the dipole slightly tilted with respect to the planetary rotation axis, and having the same polarity as that of Earth's (e.g., Connerney and Ness, 1988). Because of the limited data set provided by the two Mariner 10 fly-bys that penetrated the magnetosphere, the relative contribution to the total field by dipolar, quadrupolar, and multipolar components is highly uncertain. Indeed, Connerney and Ness (1988) showed that although the total field strength is relatively well constrained, the data allow, with little change in model error estimates, a quadrupole contribution that can be negligible or one that approaches the dipole strength.

Prior to the Mariner 10 discovery of the magnetic field it had typically been assumed that Mercury's iron core would have frozen out, precluding the possibility of an intrinsic field with a dynamo origin. More recent thermal evolution models favor a partly liquid core with a solid inner core of uncertain radius, depending primarily on the concentration of sulfur (Hauck et al., 2004; Zuber et al., 2007). Recent ground-based measurements of Mercury's libration confirm the existence of a partly molten

* Corresponding author. Fax: +1 (780) 492 0714.
E-mail address: kabin@phys.ualberta.ca (K. Kabin).
[1] Now at Carnegie Institution of Washington, DC 20005, USA.

0019-1035/$ – see front matter
doi:10.1016/j.icarus.2007.11.028

core (Margot et al., 2007), which is a necessary but not sufficient condition for dynamo action. Venus, for example, which almost certainly has a liquid core, has no intrinsic magnetic field, probably because the core thermal state yields stable stratification (e.g., Nimmo, 2002).

Although alternative explanations have been proposed, such as permanent magnetism (Aharonson et al., 2004) and thermoelectric currents (Stevenson, 1987), the Hermean magnetic field is likely to be generated by a dynamo process. Several recent dynamo simulations successfully produced weak magnetic fields which are consistent with the known constraints for Mercury (Heimpel et al., 2005; Stanley et al., 2005; Christensen, 2006; Olson and Christensen, 2006). The details of these simulations and their possible relevance to Hermean magnetosphere are discussed in Section 2. The characteristics of the internally generated magnetic field depend, however, on the core properties and geometry. Therefore, by studying Mercury's magnetosphere we can gain a valuable glimpse into the internal structure and evolution of the planet. The success of this approach, obviously, depends on our ability to separate magnetic field measured by a spacecraft into the internal field of the planet and external contributions associated with magnetospheric currents. Unfortunately, Mercury's magnetic field is weak while the IMF it interacts with along its orbit (which has a perihelion at 0.307 AU and an aphelion at 0.467 AU) is relatively strong. The solar wind dynamic pressure at Mercury's orbit on the average is also a factor of three larger than that at Earth, for example. Using the standard approximation of equating the solar wind dynamic pressure and magnetic pressure at the magnetopause, one can estimate the magnetopause current density to be proportional to $\sqrt{\rho_{SW} u_{SW}^2}/\Delta$ where ρ_{SW} is the solar wind density, u_{SW} is the solar wind speed, and Δ is the magnetopause thickness. Thus, the magnetopause current density is roughly a factor of two larger at Mercury than at Earth, as well as located much closer to the planet. Therefore, we can expect that solar wind related contributions to the magnetic field in Hermean magnetosphere are considerably larger than those at Earth, or in any other planetary magnetosphere in the Solar System.

A good summary of our pre-MESSENGER knowledge of the Hermean magnetosphere is given by Slavin (2004) and Slavin et al. (2007). It has a number of Earth-like features with a notable difference being the absence of a gravitationally bound atmosphere and, therefore, ionosphere (Killen and Ip, 1999). The magnetosphere of Mercury has been modeled on several occasions in the past. For example, Kabin et al. (2000) using an MHD model described in detail configurations of the Hermean magnetosphere for typical and fast solar wind conditions and IMF forming a 20° angle with the solar wind speed (consistent with the Parker spiral structure of the heliospheric magnetic field). A study of Mercury's magnetospheric configurations for various solar wind dynamic pressures and IMF orientation using a different MHD model was carried out by Ip and Kopp (2002) who focused on the polar cap area and its possible connection with the observed distribution of sodium in the Hermean environment (Potter et al., 1999). A more sophisticated hybrid model which includes fluid electron and particle ions for Mercury has been developed by Kallio and Janhunen (2003) who focused on the northward IMF cases and obtained a closed magnetospheric configuration for Mercury. Southward and Parker spiral IMF cases were studied with the same model in a later publication (Kallio and Janhunen, 2004). A hybrid model for Mercury's magnetosphere with higher resolution was presented by Trávníček et al. (2007). The results of the hybrid modeling are generally found to be similar to those of the MHD models.

Of all the planetary magnetospheres in the Solar System, the Hermean one is the smallest and most directly affected by the solar wind and IMF conditions. Therefore, if we want to assess the intrinsically generated magnetic field of Mercury, the paramount problem is to resolve the measured magnetic field into external and internal components. This difficulty was recognized by Giampieri and Balogh (2001), who looked at the problem of inverting the future MESSENGER magnetic field measurements in order to estimate internal field of the planet. In their work, however, Giampieri and Balogh (2001) did not include any contributions from the external sources. Adequately accounting for such external sources will certainly require extensive usage of models. First attempts at this difficult problem have been made by Korth et al. (2004), who used a scaled version of the Tsyganenko model (Tsyganenko, 1995) for the external field in estimating external effects on the anticipated magnetic field measurements along MESSENGER trajectory. Scaling a semi-empirical Tsyganenko model based on measurements for the Earth magnetosphere to a different planet is, however, always somewhat questionable. For example, lower Alfvenic Mach numbers at Mercury are expected to result in higher reconnection rates (Slavin and Holzer, 1979). Therefore, the magnetic field component perpendicular to the magnetopause at Mercury is likely to be significantly larger than that at Earth, which would require to substantial modifications to certain modules of Tsyganenko models, such as the "interconnection field" (Luhmann et al., 1998). Furthermore, Tsyganenko models do not include IMF B_x effects, which are expected to be much more important at Mercury than they are at Earth (Sarantos et al., 2001). While numerous simple empirical and analytical descriptions of the Hermean magnetospheric field are available and have been successfully used in studies of some aspects of Mercury's space environment (e.g., Delcourt et al., 2003), such models are not suitable for inferring the structure of the internal magnetic field from the satellite measurements.

In this paper we concentrate on a question which has not been yet addressed with advanced modeling—that of separating internal and external contributions to the magnetic field measured along a spacecraft orbit. Although solar wind and IMF conditions are generally quite variable, we use a steady state approach in this work since the reconfiguration times are expected to be quite small for the Hermean magnetosphere (e.g., Kabin et al., 2000) and, therefore, it may often be expected to be close to a quasi-stationary approximation. Furthermore, no solar wind monitor at Mercury will be available during the nominal duration of the MESSENGER mission.

The paper is organized as follows. Most probable dynamo scenarios for generation of Mercury's internal magnetic field are discussed in Section 2, followed by a description of the simplified internal field used in our modeling of the Hermean magnetosphere in Section 3. Section 4 contains the analysis of MESSENGER magnetic field measurements during the orbital stage, Section 5 describes the corresponding plasma measurements, and Section 6 outlines the model predictions for the three MESSENGER fly-bys of Mercury in 2008–2009. The results are summarized in the conclusions, given in Section 7.

2. Overview of dynamo modeling results for Mercury

Although the global magnetic field of Mercury is likely generated by dynamo action in the outer core of the planet, dynamo theory has difficulties in explaining a magnetic field as weak as that of Mercury. A common assumption of the dynamo theory is that rotational (Coriolis) forces are in rough balance with magnetic (Lorentz) forces in the actively convecting dynamo region (Fearn, 1998; Stevenson, 2003). This so-called magnetostrophic balance is represented qualitatively by the Elsasser number

$$\Lambda = \frac{B^2}{\rho\mu_0\eta\Omega},$$

where B is the magnetic field strength, μ_0 is the permeability of free space, ρ and η are the mass density and the magnetic diffusivity of the fluid in the source region, respectively, and Ω is the planetary rotation rate. Accounting for the fact that magnetic fields must be stronger inside the source region than outside, Elsasser numbers based on the magnetic field at the tops of the dynamos of Earth, Saturn and Jupiter are of order $\Lambda \sim 0.1$ (Stevenson, 2003; Olson and Christensen, 2006), which indicates that the magnetostrophic balance holds for the strong magnetic fields generated in the liquid metal (either iron or hydrogen) interiors of these planets.

In contrast to the strong, dominantly dipolar magnetic fields of Earth, Jupiter and Saturn, the magnetic fields of the Ice Giants, Uranus and Neptune are multipolar, nonaxisymmetric and relatively weak, with $\Lambda \sim 0.01$ (Stevenson, 2003; Olson and Christensen, 2006). The character of the magnetic fields of those planets may be explained by the low conductivity of the electrolytic "liquid ice" dynamo source region. Numerical dynamos with low conductivity fluid have been shown to yield weak multipolar fields that arise from mainly geostrophic flow which, in contrast to magnetostrophic flow, is characterized by a balance between Coriolis forces and pressure gradients (e.g., Gómez-Pérez and Heimpel, 2007).

For Mercury, the extremely low Elsasser number ($\Lambda \sim 3 \times 10^{-5}$) (Stevenson, 2003; Olson and Christensen, 2006) seems to indicate that a Hermean dynamo operates in a vastly different dynamical regime than other planetary dynamos in the Solar System. [See Christensen and Aubert (2006); Olson and Christensen (2006) for further planetary magnetic field scaling models relevant to Mercury.]

Several different types of dynamo models have been proposed to explain the weak Hermean magnetic field. A low Elsasser number multipolar dynamo regime has been shown to occur when inertia starts to dominate locally over Coriolis forces (Christensen and Aubert, 2006). Mercury's slow rotation favors this regime (Olson and Christensen, 2006). An attractive feature of the multipolar dynamo explanation is that this regime seems to occur for a wide range of parameters. However, as mentioned above, there is no strong observational evidence that Mercury's magnetic field is multipolar. In addition, three different but related models have emerged recently that can explain Mercury's weak magnetic field by invoking a regional dynamo source (Heimpel et al., 2005; Stanley et al., 2005; Christensen, 2006). In each of these models strong magnetic field is generated by a dynamo process in a region of the liquid core that takes up a fairly small fraction of the total volume, resulting in a weak global field. In the models of Stanley et al. (2005) convection and dynamo action occur in a thin shell that surrounds a large solid inner core. In a thin shell core geometry, convection is favored outside the tangent cylinder, which is defined as the imaginary cylinder tangent to the inner core equator and parallel to the rotation axis (see, e.g., Fig. 6 of Heimpel et al., 2005). Stanley et al. (2005) studied cases in which dynamo action is confined to the strongly convecting region outside the tangent cylinder. Weaker global fields then result for thinner shells in which the volume of convection and, therefore, dynamo action is relatively small. In the thick-shell models of Heimpel et al. (2005), convection and dynamo action are regionalized by the geometrical effect of a small inner core, which favors the development strong convection near the inner core boundary and in a single or regional convective plume. Christensen (2006) invokes a stably stratified region toward the top of the core in an Earth-like shell geometry such that dynamo action occurs in a small volume near the inner core boundary, yielding a very weak multipolar field at the model outer surface.

The global magnetic fields that result from different dynamo models can be distinguished by their gross characteristics (either dipolar or multipolar), by their more detailed morphologies, and by secular time variation of the magnetic field (typically, on the time-scale of years). Note, that magnetic field generated by even a multipole dynamo will still be dominated by a dipole term sufficiently far from the source region. The latitudinal spherical harmonic spectra associated with thick-shell dynamos (Heimpel et al., 2005) are typically dominated by the dipole component (spherical harmonic degree $l = 1$), with minor energy in the higher multipoles. Likewise, the azimuthal spectra typically have a strong peak at low order and exhibit strong asymmetry with respect to the azimuthal angle. In contrast, thin-shell dynamos are typically highly axisymmetric and have latitudinal spectra that drop off more slowly, with significant energy in the higher, multipolar components. Likewise, the azimuthal spectra of thin shell dynamos favor higher orders. For shell radius ratio of 0.65 studied by Heimpel et al. (2005) the dominant azimuthal harmonic order of 20 corresponds to 20 magnetic flux patches, which arise from convective plume structures that encircle the axis of rotation near the latitude where the tangent cylinder intersects the top of the dynamo. Similarly, Stanley et al. (2007) argue that it may be possible

to distinguish thin shell from thick shell core geometries from magnetic field morphologies.

Another characteristic feature that could give clues to Mercury's core geometry and dynamo behavior is the secular variation of the magnetic field. For comparison, for the Earth, which has a well-developed dipolar dynamo, the secular variation of the magnetic field magnitude is on the order of 1% per year and the rate at which the magnetic poles move is about 0.25° degrees for year. Since Mercury's core has roughly half the radius of Earth's and diffusion time scales like the radius squared, Mercury's magnetic diffusion time scale is roughly 1/4 that of the Earth. Also, since higher multipoles diffuse faster than the dipole, fast secular variation could indicate that Mercury is indeed in a multipolar dynamo regime. However, such interpretations can be complicated by the details of the core convective state. For example, in the model of Christensen (2006), the magnetic field of a deep-seated convective dynamo diffuses through a stably stratified shallower layer, which effectively acts as a low pass filter to variability in time and space, resulting in very long timescale secular variation outside the core. With MESSENGER and BepiColombo missions almost continuously monitoring Mercury's magnetic field for nearly a decade it might be possible to determine secular variations of the main field, although solar wind and IMF induced variations (discussed in Section 4) will certainly make this an extremely difficult task. However, if secular variations of the Hermean internal field can be inferred from the satellite observations, they would be most helpful in constraining the dynamo mechanism.

3. Representation of Mercury's internal magnetic field in the MHD model

Although dynamo models can provide a representation of the internal magnetic field which involves a very large number of spherical harmonics, such fields have not been used to date in many global magnetopsheric simulations. Therefore, in this paper we restrict the main field expansion to only the first two terms. The first term of the spherical harmonic expansion is the dipole field. If the dipole moment is along the z axis, then the magnetic field is given by

$$B_x = B_0\frac{3xz}{r^5}, \qquad B_y = B_0\frac{3yz}{r^5},$$
$$B_z = B_0\left(\frac{3z^2}{r^5} - \frac{1}{r^3}\right), \tag{1}$$

where (x, y, z) are the Cartesian coordinates, measured in the Mercury radii, in the system equivalent to Geocentric Solar Magnetospheric (GSM) for the Earth. Here r is the distance from the center of the planet (in Mercury radii), and B_0 is the magnetic field strength of the dipole at the equator. For Mercury, the z axis of this coordinate system coincides with the planet's rotation axis which is nearly perpendicular (within 0.02°) to Mercury's orbital plane (Blanc et al., 2005). If the dipole moment is tilted in the (x, y) plane by an angle ψ from the z axis (assumed to be positive if northern magnetic pole is tilted towards the Sun), the magnetic field is given by

$$B_x = B_0\left(\frac{3(x\sin\psi + z\cos\psi)x}{r^5} - \frac{\sin\psi}{r^3}\right),$$
$$B_y = B_0\frac{3yz}{r^5},$$
$$B_z = B_0\left(\frac{3(x\sin\psi + z\cos\psi)z}{r^5} - \frac{\cos\psi}{r^3}\right). \tag{2}$$

From Mariner 10 measurements the dipole tilt angle ψ was estimated to be about 10° (Ness et al., 1976; Connerney and Ness, 1988).

Generally, quadrupole field needs to be described by five independent parameters. In this work, however, we restrict ourselves to a symmetric quadrupole aligned with the z axis for which the magnetic field is given by

$$B_x = B_0^Q\left(\frac{5xz^2}{r^7} - \frac{x}{r^5}\right), \qquad B_y = B_0^Q\left(\frac{5yz^2}{r^7} - \frac{y}{r^5}\right),$$
$$B_x = B_0^Q\left(\frac{5z^3}{r^7} - \frac{3z}{r^5}\right). \tag{3}$$

Here, parameter B_0^Q determines the quadrupole field strength at $r = 1$. As a function of the polar angle (co-latitude) θ, measured from the z axis, quadrupole magnetic field strength at the surface of the planet is given by $B = B_0^Q\sqrt{5\cos^4\theta - 2\cos^2\theta + 1}$. Therefore, the quadrupole magnetic field strength is $2B_0^Q$ at the z axis (the pole) and B_0^Q at the equator. This makes the B_0^Q parameter convenient and similar to B_0 often used for dipole fields.

In this paper we use three models for the internal magnetic field: (i) nontilted dipole given by Eq. (1) with $B_0 = 350$ nT; (ii) tilted dipole (Eq. (2)) with $B_0 = 350$ nT and $\psi = 12°$ based on Ness et al. (1976); (iii) tilted dipole with the same parameters as before plus a quadrupole field (Eq. (3)) with $B_0^Q = 45$ nT. This value for the quadrupole strength is expected from the results of either thick or thin shell dynamo simulations (Heimpel et al., 2005; Stanley et al., 2005). Although Mariner 10 observations show that Mercury's dipole axis is most likely tilted by about 10° (Connerney and Ness, 1988), we include a model with no tilt in ours study because that is the simplest possible model for the internal field, and because most Hermean magnetospheric models to date assumed nontilted dipole (e.g., Kabin et al., 2000; Ip and Kopp, 2002; Kallio and Janhunen, 2003; Delcourt et al., 2003; Trávníček et al., 2007). Therefore, internal magnetic field model (i) is important for consistency with the earlier modeling work.

Fig. 1 shows the three components of the magnetic field in vacuum produced by these three internal magnetic field models for the three orbits considered in this work. These would represent the corresponding measurements by MESSENGER if the magnetospheric effects could be completely neglected (as it was done in the study of Giampieri and Balogh, 2001). Clearly, if this were the case, specification of the internal field model from spacecraft measurements would be straightforward. The differences in the magnetic fields resulting from different internal magnetic field models are generally larger than 20 nT near

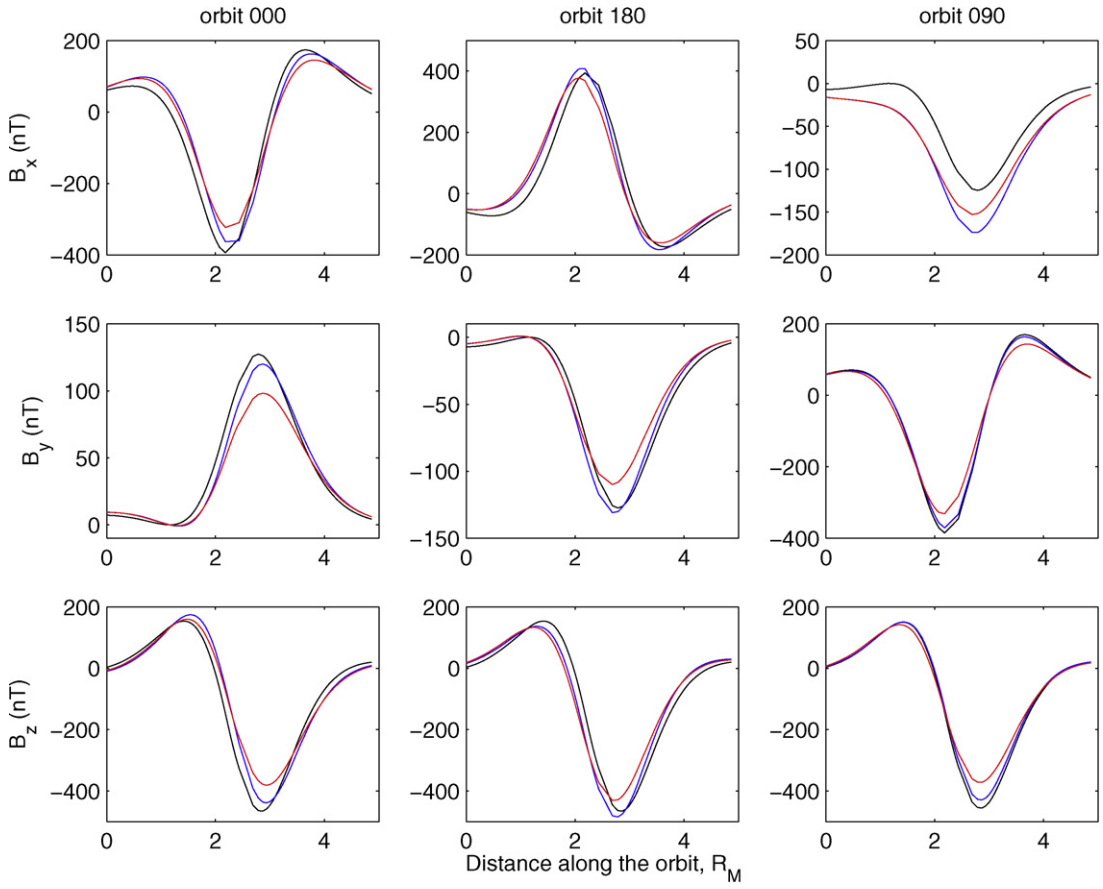

Fig. 1. Three components of the magnetic field along three different MESSENGER orbits for different internal models (no magnetosphere). Black line corresponds to nontilted dipole, blue line to tilted dipole, and red line to tilted dipole + quadrupole internal field models. (For interpretation of the references to color in this figure legend, the reader is referred to the web version of this article.)

the closest approach, and in some cases exceed 50 nT. For comparison, MESSENGER magnetometers have the best resolution of about 0.03 nT (Gold et al., 2001). As our modeling shows, however, magnetic field differences on tens of nT are associated with IMF and solar wind effects. To account for these effects we performed MHD simulations with different solar wind conditions for every internal magnetic field model used.

4. MHD modeling of MESSENGER's magnetic field measurements during the orbiting stage of the mission

In 2011, the MESSENGER spacecraft is expected to be inserted into a nearly polar orbit around Mercury with a period of 12 h and the closest approach altitude of 200 km (0.082 R_M) over the northern hemisphere of the planet. The apoapsis of the orbit is 17,633 km (7.227 R_M) and its eccentricity is 0.7396 (Santo et al., 2001). Because of the precession of MESSENGER's orbit as Mercury moves around the Sun, the closest approach location will be rotating with respect to the Sun–Mercury line, while remaining at about 60° northern latitude. For this study we selected three representative MESSENGER's orbits: an orbit with the closest approach at the local noon (in the following referred to as orbit 000), an orbit with the closest approach in the terminator plane (orbit 090), and an orbit with the closet approach at the midnight (orbit 180).

Fig. 2 shows these three typical MESSENGER orbits cutting through the simulated magnetosphere of Mercury (left panel—for northward IMF, right panel—for southward IMF; both simulations are for pure nontilted dipole internal field; see below for other simulation parameters). The color code in Fig. 2 shows the magnetic field intensity in the north–south and equatorial planes which are translucent. Although this color code does not reflect the orientation of the magnetic field, it is easy to see that the magnetic field intensity along the spacecraft tracks is different for the two simulations. Large portions of any MESSENGER orbit lies outside of the magnetopause and, therefore, are not very useful for providing restrictions on the internal magnetic field of the planet. Therefore, in the present study we only use the parts of the spacecraft trajectories which are inside 2 R_M radius from the center of Mercury. These orbital segments are shown in white in Fig. 2. These sections of MESSENGER's orbits are, for the most part, inside the magnetopause. All these sections of the spacecraft orbit have lengths of 4.867 R_M and the closest approach is achieved at the midway points of these segments of the orbit. Using the solution of Kepler's problem (e.g., Howard, 2005) we calculate that it takes the MESSENGER spacecraft 1.017 h to travel along this section of the orbit. We show that the measurements obtained on different orbits may be used to constrain various parameters characterizing the

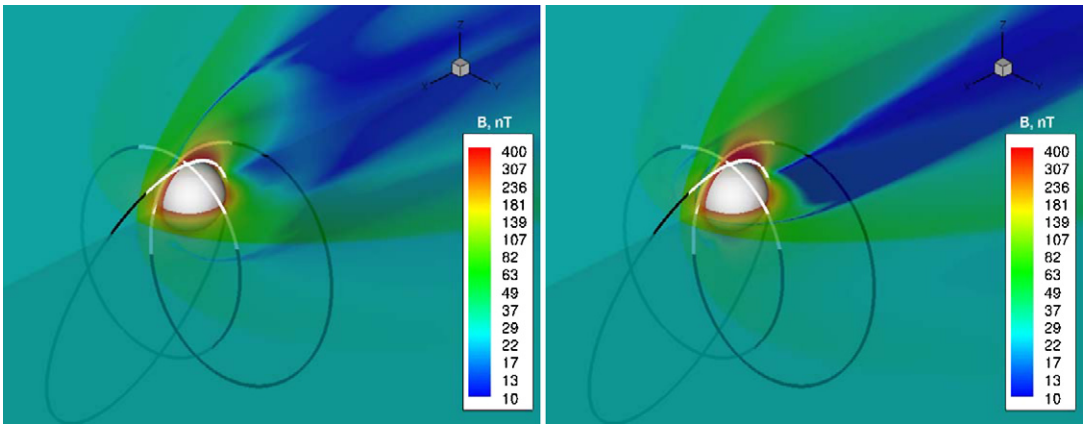

Fig. 2. Three representative MESSENGER orbits in a simulated magnetosphere: (left panel) northward IMF and nontilted dipole; (right panel) southward IMF and nontilted dipole. Sections of the orbits inside 2 R_M are shown in white. The translucent color code is the magnetic field intensity in the equatorial and north–south meridional planes.

internal field of Mercury and some of the orbits are better suited for this purpose than others.

We use the global MHD model of Kabin et al. (2000) to simulate the magnetic field in the vicinity of Mercury. For the internal magnetic field we use the three models described above, which become progressively more sophisticated. Note that the nontilted dipole model *i* is the same as the one used by Kabin et al. (2000). Compared to our previous studies here we use somewhat modified solar wind and IMF conditions, based on a recent compilation of the Helios data (Burlaga, 2001). In this paper we use a solar wind density of 40 cm^{-3}, a velocity of 430 km/s, a temperature of 50 eV, and an IMF of 25 nT (either northward, southward, or in the y direction). For every internal magnetic field model we compare results of three simulations: northward, southward, and pure B_y IMF (9 simulations total). The northward and southward IMF cases are extreme orientations of the IMF which provide the most distinct magnetospheric configurations and thus may be thought to bracket the possible variations of the magnetic field measurements due to external sources along MESSENGER trajectory. These two cases are also the most well analyzed and understood configurations of the terrestrial magnetosphere, and therefore are of modeling interest for Mercury as well for comparative magnetospheric studies. Pure IMF B_y orientation gives a magnetospheric configuration which is in some ways intermediate between those for pure northward and pure southward cases. Considering these IMF conditions gives us a good estimation for the level of variation expected in the fields measured by MESSENGER. Even though small IMF variations around the nominal Parker spiral will lead to smaller differences in the magnetic field along the spacecraft orbit, numerous other effects will be contributing to the measurements in reality (such as changes in solar wind dynamic pressure and other plasma parameters, solar wind turbulence, etc.). Since at present we cannot adequately account for all other variations affecting the measurements, we feel that differences between northward, southward, and IMF B_y orientations provide reasonable estimations for the differences in external fields we can expect in the vicinity of Mercury.

Figs. 3, 4, and 5 show variations of the B_x, B_y, and B_z components of the magnetic field, respectively, in the modeled Hermean magnetosphere along MESSENGER trajectories 000, 090, and 180 (orbits 000 and 180 are close to the north–south meridional plane, while 090 is close to the terminator plane) inside 2 R_M (the section shown in white in Fig. 2). In all these figures, solid lines correspond to the northward IMF, dashed lines to the southward IMF, and dotted lines to pure IMF B_y cases. Different colors are used to distinguish different internal magnetic field models: blue corresponds to the pure nontilted dipole (*i* model), red to the tilted dipole (*ii* model), and green to the tilted dipole with quadrupole contribution (*iii* model). The horizontal axes at the top of the plots show the spacecraft time (in minutes) with zero corresponding to the closest approach. For the considered section of the orbit there is an almost linear proportionality between time and distance along the spacecraft track. Note that because the limits of variation of the same magnetic component for different orbits can be quite different, the scales for the panels of Figs. 3, 4, and 5 are different as well. The sudden jump in the B_y component seen for the dotted lines in Fig. 4 is associated with the magnetopause crossing: for the IMF B_y case there is a strong B_y component in the magnetosheath, while for the other IMF orientations considered in the present work, there is not. Similarly, the discontinuities in the B_z component of the magnetic field for southward IMF and IMF B_y configurations seen in Fig. 5 are also magnetopause crossings. For southward and B_y IMF the direction of the magnetic field changes across the day-side magnetopause (making it obvious in the plots of B_z), while for northward IMF it does not (so the magnetopause does not appear as obviously in the magnetic field plots, and has to be identified from other parameters, see Section 5).

Ideally, in order to separate different internal magnetic field models, we would like to see solid, dashed and dotted lines of the same color in Figs. 3, 4, and 5 being close together and well distanced from the lines of different color. If that were the case, the IMF effects would be quite small, and the magnetic field measured well inside the magnetosphere would be essentially the internal field of the planet. Unfortunately, Figs. 3, 4, and 5 present a different picture: the differences due to the external fields can be just as large as the differences associated with various internal field models. This is particularly true for the

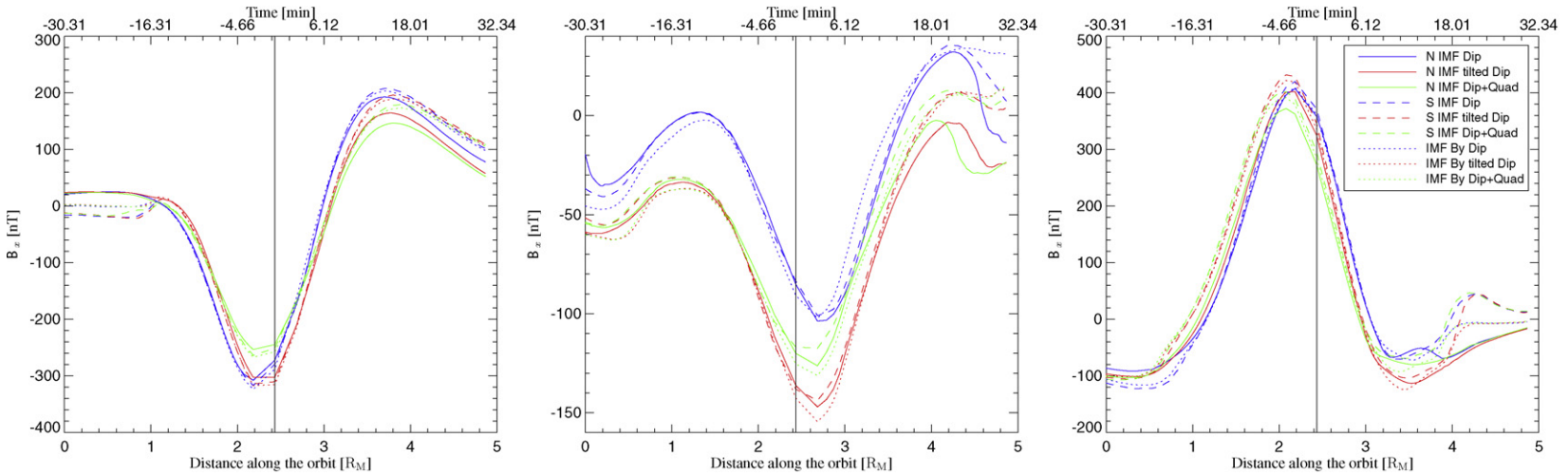

Fig. 3. B_X components of the magnetic field along MESSENGER orbit for different internal and IMF models. Left panel: orbit 000; center panel: orbit 090; and right panel: orbit 180. The vertical line marks the closest approach. The horizontal axes at the bottom of the plots show the distance along the orbit, and the horizontal axes at the top show the spacecraft time in minutes, zeroed on the closest approach.

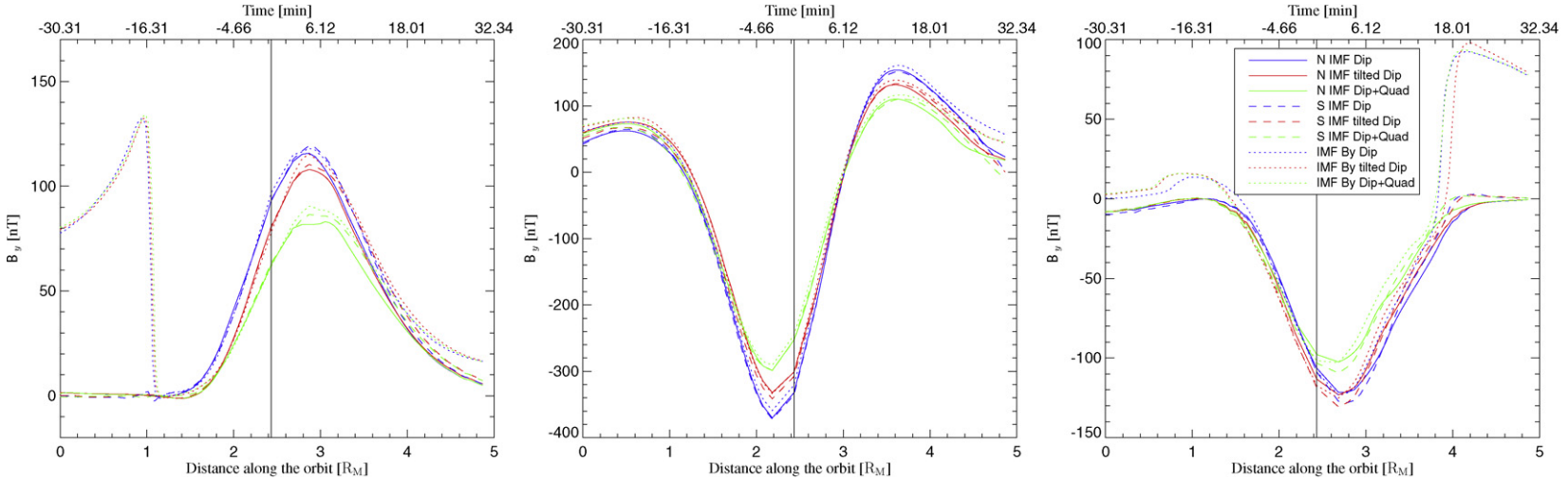

Fig. 4. B_y components of the magnetic field along MESSENGER orbit for different internal and IMF models. Left panel: orbit 000; center panel: orbit 090; and right panel: orbit 180. The vertical line marks the closest approach. The horizontal axes at the bottom of the plots show the distance along the orbit, and the horizontal axes at the top show the spacecraft time in minutes, zeroed on the closest approach.

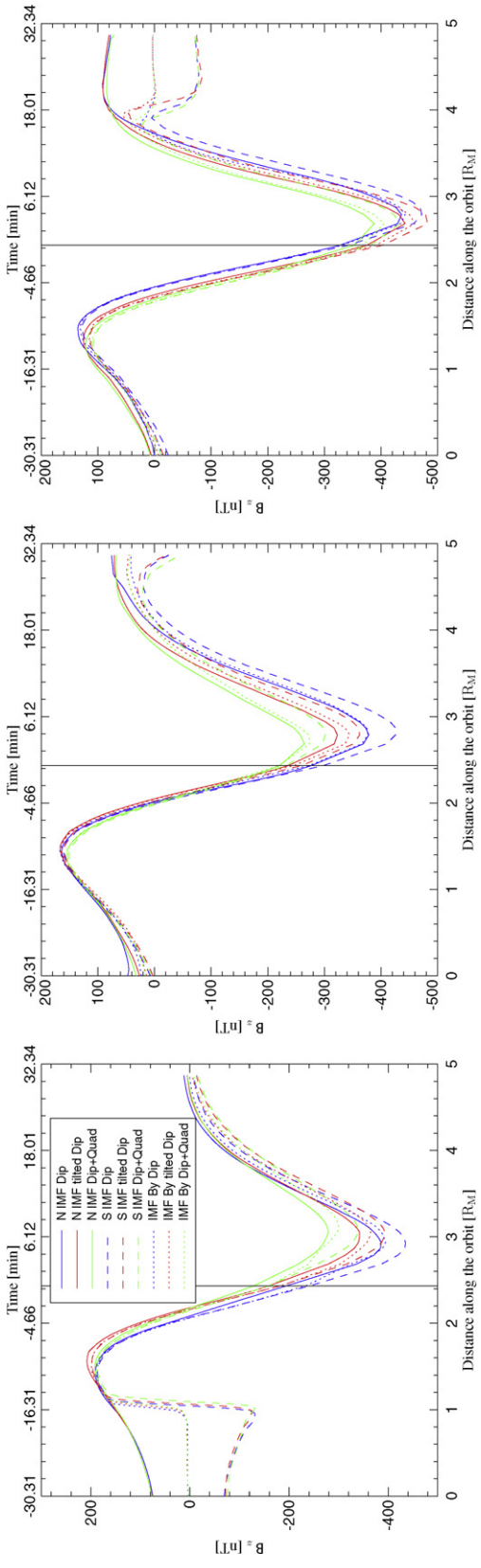

Fig. 5. B_z components of the magnetic field along MESSENGER orbit for different internal and IMF models. Left panel: orbit 000; center panel: orbit 090; and right panel: orbit 180. The vertical line marks the closest approach. The horizontal axes at the bottom of the plots show the distance along the orbit, and the horizontal axes at the top show the spacecraft time in minutes, zeroed on the closest approach.

right panels of Figs. 3, 4, and 5, which correspond to orbit 180 with closest approach on the night-side of Mercury. For this orbit the B_x component of the magnetic field provides no basis for distinguishing internal field models, the B_y component shows some difference for models with and without dipole tilt, but no difference between the models with and without quadrupole field. The B_z component for this orbit, once again is hardly useful at all for specifying the internal field of Mercury. Furthermore, as Fig. 5 shows, the differences between different internal field models are particularly small in the B_z component, which is the dominant internal magnetic field component, and therefore, could have been expected to provide the best results for determining the internal magnetic field model. The differences between the various internal magnetic field models, however, are quite pronounced in the B_y component of simulated magnetic field shown in the left panel of Fig. 4 (orbit 000) and are achieved near the closest approach rather than near the peak of the B_y component. In contrast as appears from Fig. 5 for the B_z, some of the internal field models are better separated at the location of the largest B_z magnitude, rather than at the closest approach. The separation between different internal field models is particularly good for the B_x component for orbit 090 as seen in the center panel of Fig. 3. This trajectory and magnetic field component seem to be most well suited for determining the dipole tilt angle, as the differences between models with and without dipole tilt are very large (on the order of 40 nT) and consistent for much of the length of the selected segment of the orbit. Thus, specifying the internal magnetic field for Mercury from MESSENGER data is a complicated task which will require an analysis of all the three components of the measured magnetic field and data taken on different trajectories of the spacecraft.

Magnetic field in the vicinity of Mercury is certainly not a simple superposition of the IMF and internal field of the planet. Changing the internal field of Mercury modifies the magnetospheric current systems in nonlinear fashion resulting in a complicated interaction pattern. It is, however, interesting to what extent the roughly 10% quadrupole field affects the global configuration of the magnetosphere and the magnetic field measurements along the MESSENGER orbit. Fig. 6 shows the results of a subtraction of the magnetic field for the simulations with internal field (ii) (tilted dipole) from those with internal field (iii) (tilted dipole and quadrupole). Red lines corresponds to the northward IMF, blue lines to southward IMF, and green lines to pure B_y cases. The black line in Fig. 6 shows for comparison the pure quadrupole field. Clearly, all the lines in all the three figures are close to each other, thus implying that the nonlinear part of the response of the Hermean magnetosphere to the addition of the 10% quadrupole to the internal field is relatively small, and that most of the nonlinearity of the system is accounted for by the interaction of the tilted dipole with the solar wind. Large differences at about $s = 1\ R_M$ (s is the distance along the orbit) are associated with the small change in magnetopause locations for the models with and without the quadrupole component, and the fact that magnetic field is generally discontinuous across the day-side magnetopause. The difference between the different lines in these figures is particu-

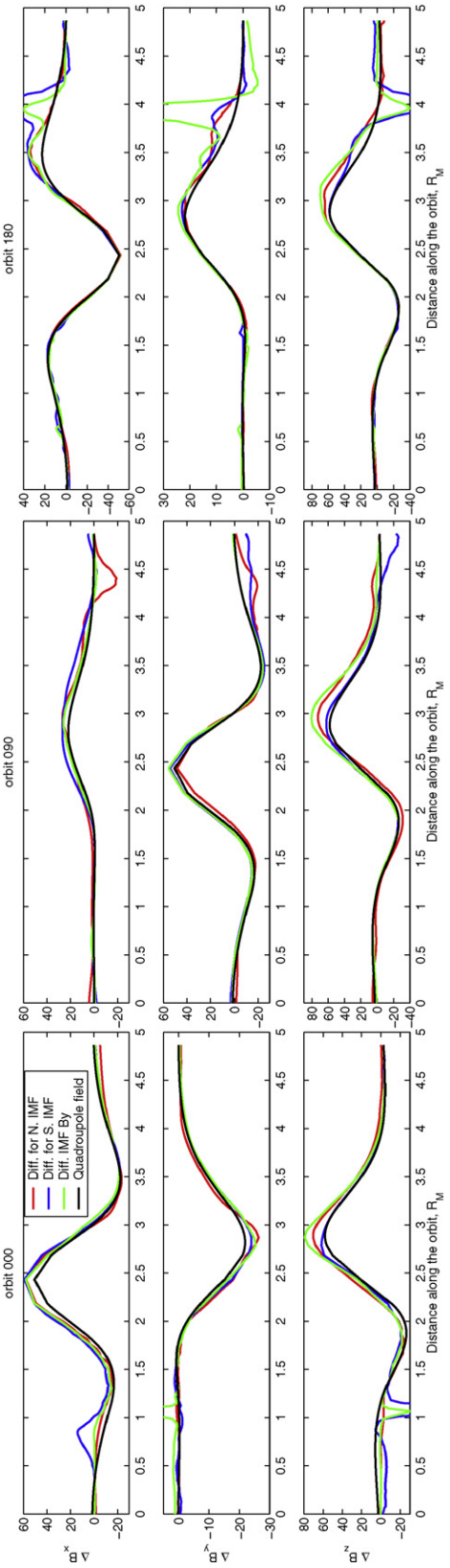

Fig. 6. Difference between the simulations with and without quadrupole component of the internal field [internal field *iii* and *ii* along MESSENGER orbit 000 (left panel), orbit 090 (center panel), and orbit 180 (right panel)]. Results for northward IMF are shown with red lines, southward IMF with blue, and pure B_y IMF with green. Black lines correspond to the pure quadrupole field. (For interpretation of the references to color in this figure legend, the reader is referred to the web version of this article.)

larly small on the flank which is furthest from the magnetopause (and, therefore, the currents associated with it). Thus, one can imagine the following procedure for determining the higher-order harmonics for Mercury. First, the dipole strength and tilt are determined, after that a simulation with this internal magnetic field is run and a quadrupole field is fitted, as if in vacuum, to minimize the variance between the results of this simulation and the measurements. The final step of this approach can, in essence, follow the procedure of Giampieri and Balogh (2001).

It is useful to assess the strength of the external fields along MESSENGER orbit which are produced by magnetospheric current systems. To this end, Fig. 7 shows the result of subtraction of the internal field contribution from the total field computed by in the MHD model. All plots are for the simulation with internal magnetic field model *iii*: tilted dipole + quadrupole. Blue line corresponds to the northward IMF conditions, red line to southward IMF conditions, and green line to pure IMF B_y case. Fig. 7 shows that magnetospheric currents can contribute more than 100 nT to the measured magnetic field along MESSENGER orbit. The difference between the external fields computed for different IMF conditions is, however, somewhat smaller, but still can be as large as 50 nT in some components. Therefore, our simulations suggest that higher-order terms Mercury's internal field which contribute less than few tens of nT along the MESSENGER trajectory most likely will not be detected over the noise introduced by the changes in the magnetospheric current system of the Hermean magnetosphere. Considering that high-order contributions to the magnetic field decay very rapidly with distance, spherical harmonics of the order ~20 would probably not produce identifiable magnetic fields along MESSENGER orbit. Thus, it appears unlikely that MESSENGER will provide magnetic field data of sufficient detail to confirm the existence of a thin shell dynamo, as described in Section 2. However, numerous orbital passes through the polar regions of the Hermean magnetosphere should be enough to detect localized strong asymmetric patches of the magnetic flux suggested by the thick dynamo scenario. This mechanism for generating the internal field of Mercury, therefore, may be either supported or disproved by the observations during the orbital stage of the mission.

5. Modeling the plasma parameters along MESSENGER's orbit

MHD modeling allows to make predictions with regard to not only magnetic field, but some plasma parameters as well. For example, Fig. 8 shows plasma density along the same three sections of MESSENGER's orbits as were used for magnetic field studies. In all the nine simulations, the magnetopause is found at approximately the same location (around $s = 1$) for orbit 000 (top panel of Fig. 8), however the density gradient across the magnetopause is much larger in the case of southward and B_y IMF than for northward IMF. A density peak observed in all models between $s = 2$ and 3 R_M is associated with the magnetospheric plasma flow into the cusp area. The exact location of this peak depends on the IMF orientation as well as on the tilt of dipole, but is not influenced to any significant degree by

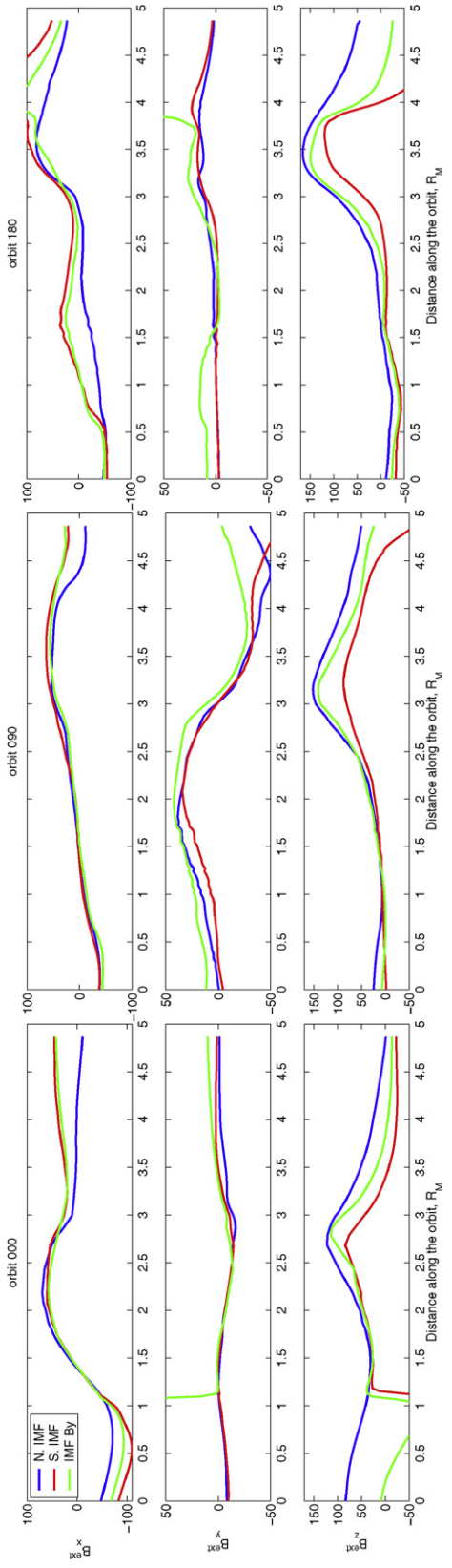

Fig. 7. External contribution to the magnetic field along MESSENGER orbits. Blue line corresponds to the northward IMF conditions, red line to southward IMF conditions, and green line to pure IMF B_y case. (For interpretation of the references to color in this figure legend, the reader is referred to the web version of this article.)

the quadrupole moment. Thus, plasma density along orbit 000 can be used as an additional parameter to constrain the internal magnetic field model for Mercury, in particular the dipole tilt. On the other hand, plasma density along the terminator orbit 090 is much more affected by the IMF and solar wind conditions than by the internal field models, and therefore, can provide little additional information. The same is, unfortunately, true with respect to orbit 180. Note, that the selected sections of the orbit, which are most relevant to estimations of the internal magnetic field of Mercury, do not extend to the equatorial plane, and, therefore, plasma density increases associated with the plasma sheet do not appear in Fig. 8.

6. Modeling of MESSENGER fly-bys of Mercury

Before being inserted into the orbit, MESSENGER spacecraft will perform 3 fly-bys of Mercury on January 14, 2008, October 6, 2008, and September 29, 2009. All of them occur on the dusk flank of the Hermean magnetosphere, but as follows from the orbital dynamics of Mercury, the first and the third fly-bys would have their closest approaches separated by nearly 180° longitude in Mercury fixed longitude. The third fly-by corresponds to a longitude which is about 30° different from that of the second fly-by. Thus, the geometry of the fly-bys allows a very wide coverage in Mercury-fixed longitude and is very promising for determining nonaxisymmetric contributions to the internal magnetic field of the planet.

The trajectories of these fly-bys are shown in Fig. 9 which uses an MHD simulation for the northward IMF and internal field (i) (nontilted dipole) as a background. Only the sections of the fly-by trajectories which are inside 3 R_M are shown; these are the sections of trajectory which are used in the following analysis. It should be noted that the usefulness of the magnetic field measurements taken during these fly-bys depends to some extent on how steady the solar wind and magnetospheric conditions will happen to be at the time of the fly-bys. For example, most of the data from the first fly-by of Mercury by Mariner 10 on March 29, 1974 are not very useful for inferring its magnetic field because of the rapid (and unknown) changes of the solar wind and IMF conditions.

Figs. 10, 11, and 12 show the three components of the magnetic field extracted along the three fly-bys of Mercury. As compared to the similar plots for the orbiting stage of the mission (Figs. 3, 4, and 5) variations associated with either the different internal field models or with different solar wind conditions are very large in the B_x and B_z components, but are not nearly as prominent in the B_z component (which is by far the largest of the three components). This is a result of sampling a different part of the magnetosphere by the fly-bys (which are all close to the equatorial plane) as compared to the orbits (which provide more information about the high-latitude regions). Clearly, the B_z component is the least useful in distinguishing the different internal magnetic field models, except for fly-by 1 (left panel of Fig. 12). For this fly-by, the B_z component shows modest difference (at the field peak location, rather than at the closest approach) associated with the various internal field models

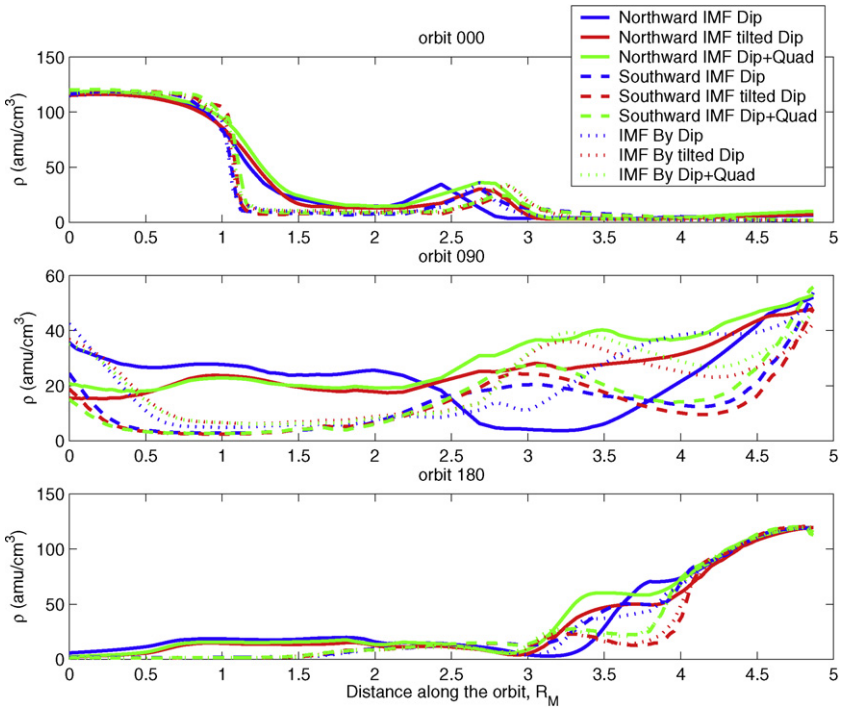

Fig. 8. Plasma density along the spacecraft trajectory for the different simulations.

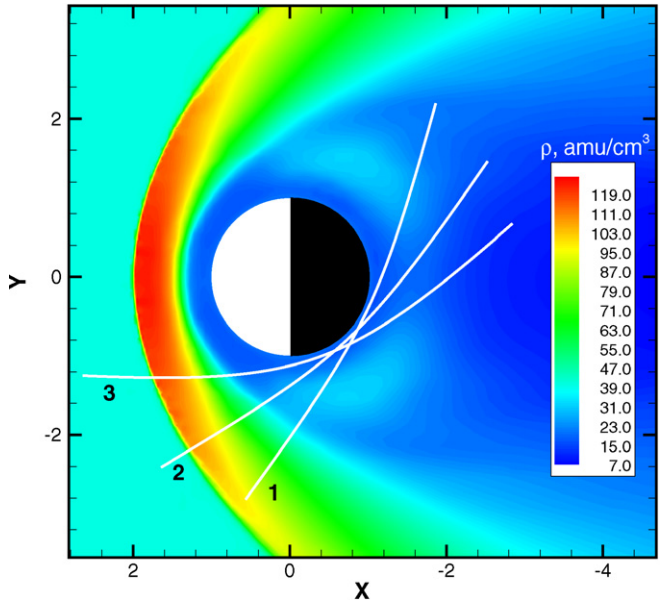

Fig. 9. Projections (along the z axis) of the three MESSENGER fly-bys on the equatorial plane. Only the sections of the fly-by trajectories inside a radius of 3 R_M from the center of the planet are shown.

which is, nevertheless consistently larger than solar wind induced perturbations of the field.

Similarly to the B_x for orbit 090 (Fig. 3, central plane) Figs. 10, 11 show a very large difference for the models with dipole tilt and without dipole tilt (blue lines are quite far from the red and green lines). This gives confidence that using a combination of magnetic field measurements taken during the fly-bys and for the orbits close to the terminator plane the parameters of the dipole component of the internal magnetic field can be evaluated quite accurately. As it is discussed in the end of Section 4 the dipole strength and its tilt are responsible for much of the nonlinear response of the magnetospheric current systems to the internal field parameters. It is, therefore, essential to use as accurate as possible estimations for these parameters in combination with modeling in order to attain information about higher harmonic contributions to Mercury's internal field.

Similarly to the figures for the orbital part of the mission, magnetopause crossings can be clearly seen in Figs. 10, 11 at the points where the magnitude of the magnetic field components changes rapidly. They occur at about $s = 4.6$ for fly-by 1, $s = 4.3$ for fly-by 2, and $s = 4.2$ for fly-by 3.

Although the magnetic field variations associated with IMF conditions are generally as large in magnitude as the variations associated with the internal field models in Figs. 10 and 11 they have different variation along the fly-by path. Therefore, if the solar wind and IMF conditions are known (e.g., can be assumed to be similar to those at the time when MESSENGER was still outside the Hermean magnetosphere) MHD modeling can be effectively used to distinguish internal contribution to the magnetic field measurements. The three fly-bys of Mercury represent a more promising opportunity for this study as compared with the orbital part of MESSENGER mission. Although sometimes Figs. 3, 4, and 5 show as much difference in nT between different simulations as Figs. 10, 11, and 12, the variation of the field along the trajectory during the orbital stage is generally very similar for all internal field models and IMF conditions. In contrast, for the fly-bys our MHD model predicts more distinction in the character of the magnetic field variation along the trajectory, which should aid in interpretation of the results. Thus, despite the much larger volume of measurements taken

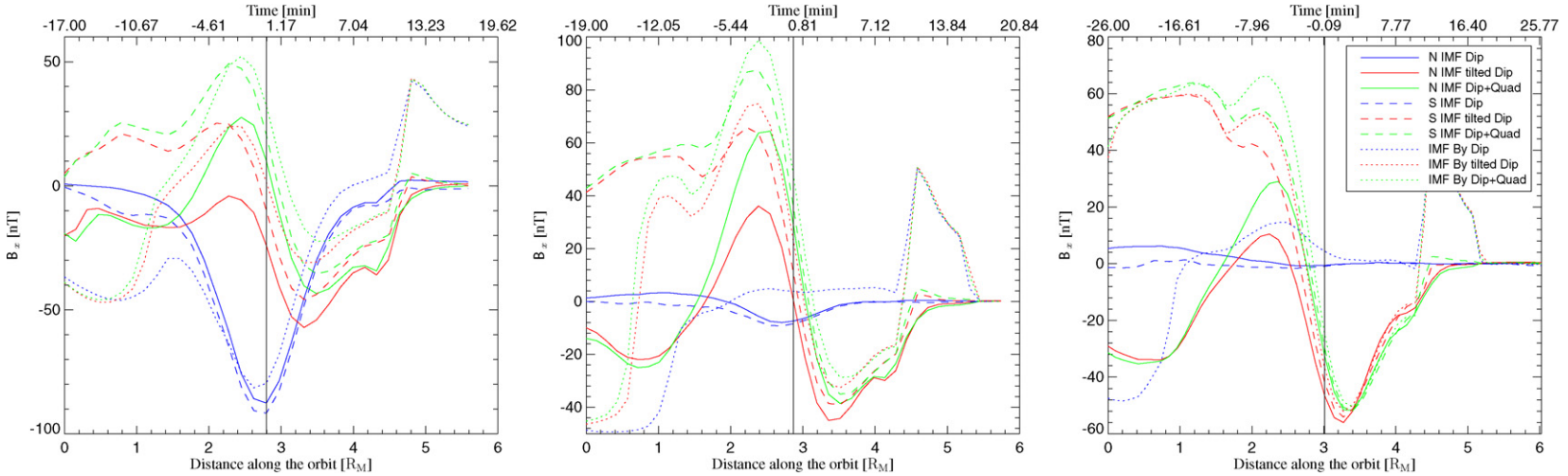

Fig. 10. B_x components of the magnetic field for the three MESSENGER fly-bys of Mercury. The vertical line marks the closest approach. Left panel is for the first fly-by, middle—for the second, and right—for the third. The horizontal axes at the bottom of the plots show the distance along the fly-by trajectory and the horizontal axes at the top show the spacecraft time in minutes, zeroed on the closest approach.

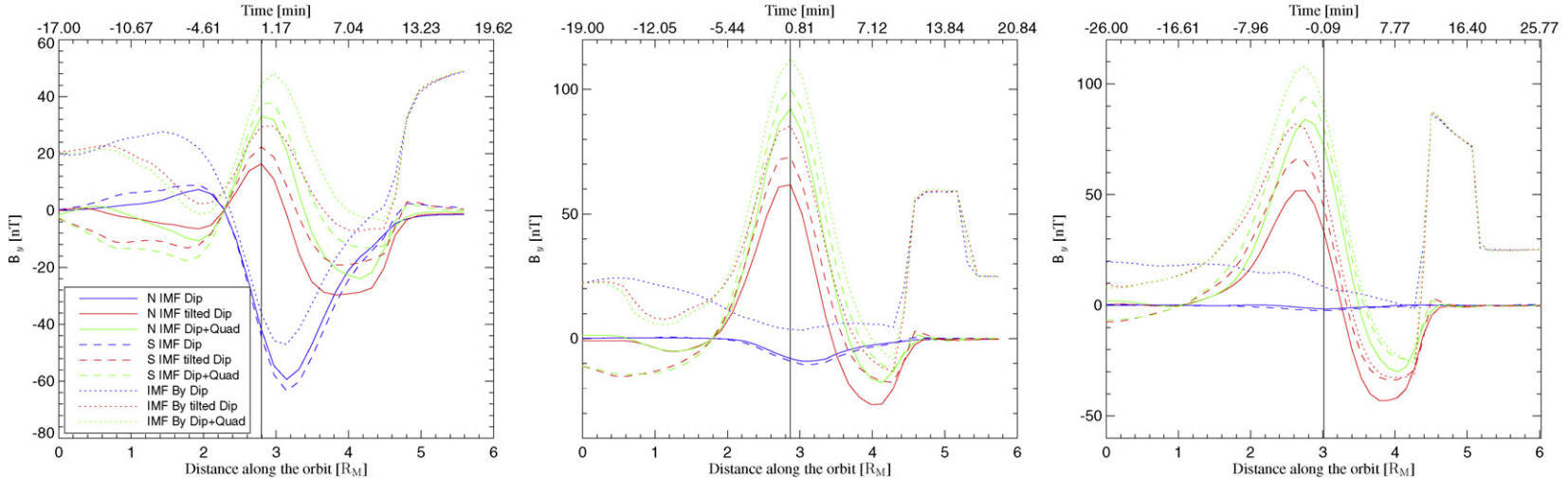

Fig. 11. B_y components of the magnetic field for the three MESSENGER fly-bys of Mercury. The vertical line marks the closest approach. Left panel is for the first fly-by, middle—for the second, and right—for the third. The horizontal axes at the bottom of the plots show the distance along the fly-by trajectory and the horizontal axes at the top show the spacecraft time in minutes, zeroed on the closest approach.

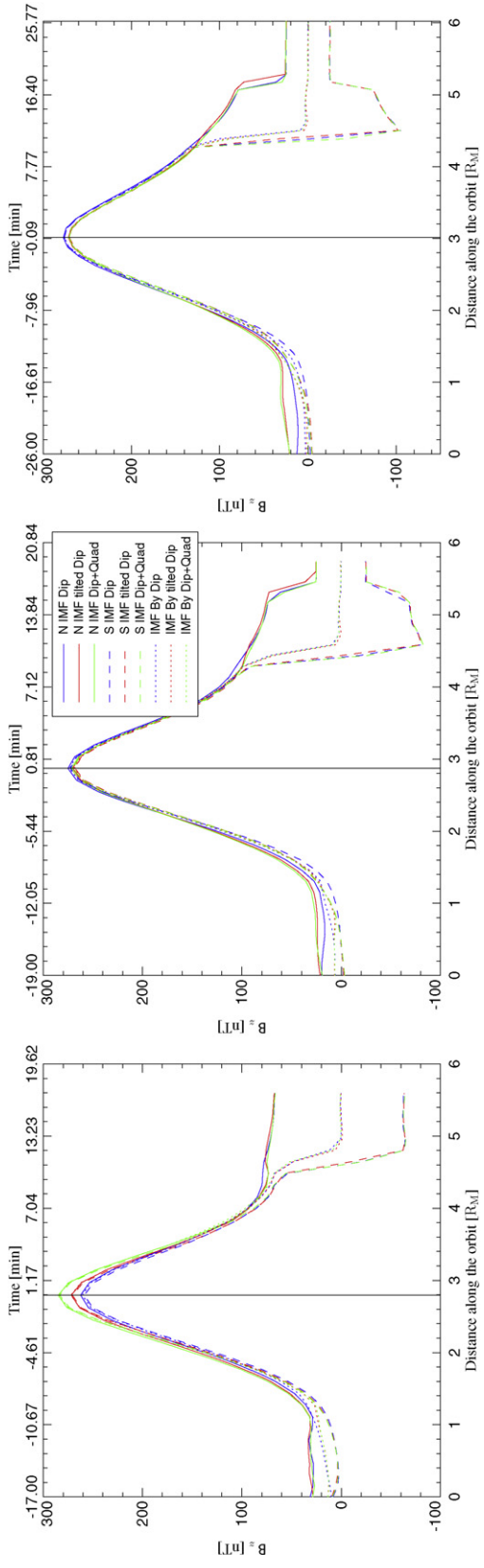

Fig. 12. B_z components of the magnetic field for the three MESSENGER fly-bys of Mercury. The vertical line marks the closest approach. Left panel is for the first fly-by, middle—for the second, and right—for the third. The horizontal axes at the bottom of the plots show the distance along the fly-by trajectory and the horizontal axes at the top show the spacecraft time in minutes, zeroed on the closest approach.

during the orbiting stage of MESSENGER mission, the information coming from the initial fly-bys may be crucial for determining the parameters of Mercury's internal magnetic field. Global modeling of the Hermean magnetosphere would have been much more reliable if a solar wind monitor were available during the fly-bys. Unfortunately, this would not be the case in 2008–2009, at the time of MESSENGER fly-bys.

7. Conclusions

In this paper we have discussed some of the problems associated with extracting information about internal magnetic field of Mercury from the MESSENGER spacecraft measurements. Of all magnetospheres in the Solar System, the Hermean one is the most strongly affected by the solar wind and IMF effects. This fact complicates the separation of a spacecraft magnetic field measurements into internal and external components. Generally, for the expected MESSENGER trajectories, which come to within 200 km of the surface of the planet, the disturbances originating from the solar wind can be as large as the expected quadrupole contribution even at the closest approach. The same holds for the three fly-bys of Mercury which are scheduled to take place before the orbital insertion. We find, however, that the initial fly-bys (which are close to the equatorial plane) generally provide a better basis for determining the parameters of a dipole component of the internal field than the later polar orbits. However, the B_x variation along a terminator trajectory also gives a very good estimation of the dipole tilt angle. In addition, the B_y component of the magnetic field for the noon-midnight orbit with the closest approach on the day-side was found to have the cleanest separation between the three internal magnetic field models. This magnetic field component also provides a fair separation for different internal field models for the terminator orbit. In contrast, all magnetic field components for the orbits close to the noon–midnight plane with periapsis on the night side of the planet appear to be much less useful for constraining the internal field. Global MHD models of Mercury's magnetosphere are capable, in principle, of calculating the external contributions to the magnetic fields, however, they require solar wind input. Unless both MESSENGER and BepiColombo are at Mercury at the same time (which would require one of the missions to be extended, and the other to be on schedule) such information will not be available. Multi-satellite observations at Mercury would have allowed the elimination of some of the most nagging uncertainties associated with using global modeling to infer the internal magnetic properties of the planet. Without such observations, however, the number of MESSENGER orbits useful for accurate determination of the internal magnetic field would be limited to those for which solar wind and IMF conditions did not change significantly while the satellite was inside the magnetosphere.

Our MHD model shows that although the magnetic field in the vicinity of Mercury changes nonlinearly with the internal field parameters, much of this nonlinearity can be accounted for by the interaction of tilted dipole with the solar wind. The dipole parameters, however, can be reliably estimated from the measurements taken during initial fly-bys and later at the orbits

passing close to the terminator plane. Once this part of the interaction is accounted for through modeling, higher harmonics of the internal magnetic field can be computed with good accuracy using relatively simple linear fitting techniques.

Because of the large magnetic field variations in the Hermean magnetosphere associated with solar wind and IMF conditions it appears unlikely that MESSENGER mission will be capable of specifying Mercury's internal field beyond degree and order of about 3. However, detection or absence of strong regional patches of magnetic flux should provide enough evidence to test available dynamo models, thus contributing to our knowledge of the interior structure of the planet.

Acknowledgments

This work is supported by the Canadian Space Agency, by Natural Sciences and Engineering Research Council of Canada, including NSERC Discovery Grant awarded to J.C. Samson, and by NASA, Contract NASW-00002 (T.Z.H.), NSF ATM 0642309 and NASA NNX07AC16G. We also acknowledge the use of WestGRID computational resources.

References

Aharonson, O., Zuber, M.T., Solomon, S.C., 2004. Crustal remanence in an internally magnetized nonuniform shell as a possible source for Mercury's magnetic field? Earth Planet. Sci. Lett. 218, 261–268.

Blanc, M., Kallenbach, R., Erkaev, N.V., 2005. Solar System magnetospheres. Space Sci. Rev. 116, 227–298.

Burlaga, L.F., 2001. Magnetic fields and plasmas in the inner heliosphere: Helios results. Planet. Space Sci. 49, 1619–1627.

Christensen, U.R., 2006. A deep dynamo generating Mercury's magnetic field. Nature 444, 1056–1058.

Christensen, U.R., Aubert, J., 2006. Scaling properties of convection-driven dynamos in rotating spherical shells and application to planetary magnetic fields. Geophys. J. Int. 166, 97–114.

Connerney, J.E.P., Ness, N.F., 1988. Mercury's magnetic field and its interior. In: Vilas, F., Chapman, C.R., Matthews, M.S. (Eds.), Mercury. Univ. of Arizona Press, Tucson, pp. 494–513.

Delcourt, D.C., Grimald, S., Leblanc, F., Berthelier, J.-J., Millilo, A., Mura, A., Orsini, S., Moore, T.E., 2003. A quantitative model of the planetary Na^+ contribution to Mercury's magnetosphere. Ann. Geophys. 21, 1723–1736.

Fearn, D.R., 1998. Hydromagnetic flows in planetary cores. Rep. Prog. Phys. 61, 175–235.

Giampieri, G., Balogh, A., 2001. Modeling of magnetic field measurements at Mercury. Planet. Space Sci. 49, 1637–1642.

Gold, R.E., Solomon, S.C., McNutt, R.L., Santo, A.G., Abshire, J.B., Acuña, M.H., Afzal, R.S., Anderson, B.J., Andrews, G.B., Bedini, P.D., Cain, J., Cheng, A.F., Evans, L.G., Feldman, W.C., Follas, R.B., Gloeckler, G., Goldsten, J.O., Hawkins, S.E., Izenberg, N.R., Jaskulek, S.E., Ketchum, E.A., Lankton, M.R., Lohr, D.A., Mauk, B.H., McClintock, W.E., Murchie, S.L., Schlemm, C.E., Smith, D.E., Starr, R.D., Zurbuchen, T.H., 2001. The MESSENGER mission to Mercury: Scientific payload. Planet. Space Sci. 49, 1467–1479.

Gómez-Pérez, N.G., Heimpel, M.H., 2007. Numerical models of zonal flow dynamos: An application to the ice giants. Geophys. Atrophys. Fluid Dyn. 101, 371–388.

Hauck, S.A.I., Dombard, A.J., Phillips, R.J., Solomon, S., 2004. Internal and tectonic evolution of Mercury. Earth Planet. Sci. Lett. 222, 713–728.

Heimpel, M.H., Aurnou, J.M., Al-Shamali, F.M., Gómez-Pérez, N., 2005. A numerical study of dynamo action as a function of spherical shell geometry. Earth Planet. Sci. Lett. 236, 542–557.

Howard, C.D., 2005. Orbital Mechanics for Engineering Students. Elsevier, Amsterdam.

Ip, W.-H., Kopp, A., 2002. MHD simulations of the solar wind interaction with Mercury. J. Geophys. Res. 107, doi:10.1029/2001JA009171.

Kabin, K., Gombosi, T.I., DeZeeuw, D.L., Powell, K.G., 2000. Interaction of Mercury with the solar wind. Icarus 143, 397–406.

Kallio, E., Janhunen, P., 2003. Modeling the solar wind interaction with Mercury by a quasi-neutral hybrid model. Ann. Geophys. 21, 2133–2145.

Kallio, E., Janhunen, P., 2004. The response of the Hermian magnetosphere to the interplanetary magnetic field. Adv. Space Res. 33, 2176–2181.

Killen, R.M., Ip, W.-H., 1999. The surface-bounded atmospheres of Mercury and the Moon. Rev. Geophys. 37, 361–406.

Korth, H., Anderson, B.J., Acuña, M.H., Slavin, J.A., Tsyganenko, N.A., Solomon, S.C., McNutt, R.L., 2004. Determination of the properties of Mercury's magnetic field by the MESSENGER mission. Planet. Space Sci. 52, 733–746.

Luhmann, J.G., Russell, C.T., Tsyganenko, N.A., 1998. Disturbances in Mercury's magnetosphere: Are the Mariner 10 "substorms" simply driven? J. Geophys. Res. 103, 9113–9119.

Margot, J.-L., Peale, S.J., Jurgens, R.F., Slade, M.A., Holin, I.V., 2007. Large longitude libration of Mercury reveals a molten core. Science 316, 710–714.

McNutt, R.L., Solomon, S.C., Grard, R., Novara, M., Mukai, T., 2004. An international program for Mercury exploration: Synergy of MESSENGER and BepiColombo. Adv. Space Res. 33, 2126–2132.

Ness, N.F., Behannon, K.W., Lepping, R.P., Whang, Y.C., 1976. Observations of Mercury's magnetic field. Icarus 28, 479–488.

Nimmo, F., 2002. Why does Venus lack a magnetic field? Geology 30, 987–990.

Olson, P., Christensen, U.R., 2006. Dipole moment scaling for convection-driven planetary dynamos. Earth Planet. Sci. Lett. 250, 561–571.

Potter, A.E., Killen, R.M., Morgan, T.H., 1999. Rapid changes in the sodium exosphere of Mercury. Planet. Space Sci. 47, 1441–1448.

Santo, A.G., Gold, R.E., McNutt, R.L., Solomon, S.C., Ercol, C.J., Farquhar, R.W., Hartka, T.J., Jenkins, J.E., McAdams, J.V., Mosher, L.E., Persons, D.F., Artis, D.A., Bokulic, R.S., Conde, R.F., Dakermanji, G., Goss, M.E., Haley, D.R., Heeres, K.J., Maurer, R.H., Moore, R.C., Rodberg, E.H., Stern, T.G., Wiley, S.R., Williams, B.G., Yen, C.L., Peterson, M.R., 2001. The MESSENGER mission to Mercury: Spacecraft and mission design. Planet. Space Sci. 49, 1481–1500.

Sarantos, M., Reiff, P.H., Hill, T.W., Killen, R.M., Urquhart, A.L., 2001. A B_x interconnected magnetosphere model for Mercury. Planet. Space Sci. 49, 1629–1635.

Slavin, J.A., 2004. Mercury's magnetosphere. Adv. Space Res. 33, 1859–1874.

Slavin, J.A., Holzer, R.E., 1979. The effect of erosion on the solar wind stand-off distance at Mercury. J. Geophys. Res. 84, 2076–2082.

Slavin, J.A., Krimigis, S.M., Acuña, M.H., Anderson, B.J., Baker, D.N., Koehn, P.L., Korth, H., Livi, S., Mauk, B.H., Solomon, S.C., Zurbuchen, T.H., 2007. MESSENGER: Exploring Mercury's magnetosphere. Space Sci. Rev. 131, 133–160.

Solomon, S.C., McNutt, R.L., Gold, R.E., Acuña, M.H., Baker, D.N., Boynton, W.V., Chapman, C.R., Cheng, A.F., Gloeckler, G., Head, J.W., Krimigis, S.M., McClintock, W.E., Murchie, S.L., Peale, S.J., Phillips, R.J., Robinson, M.S., Slavin, J.A., Smith, D.E., Strom, R.G., Trombka, J.I., Zuber, M.T., 2001. The MESSENGER mission to Mercury: Scientific objectives and implementation. Planet. Space Sci. 49, 1445–1465.

Stanley, S., Bloxham, J., Hutchison, W.E., Zuber, M.T., 2005. Thin shell dynamo models consistent with Mercury's weak observed field. Earth Planet. Sci. Lett. 234, 27–38.

Stanley, S., Zuber, M.T., Bloxham, J., 2007. Using reversed magnetic flux spots to determine a planet's inner core size. Geophys. Res. Lett. 34, doi:10.1029/2007GL030892.

Stevenson, D.J., 1987. Mercury's magnetic field: A thermoelectric dynamo? Earth Planet. Sci. Lett. 82, 114–120.

Stevenson, D.J., 2003. Planetary magnetic fields. Earth Planet. Sci. Lett. 208, 1–11.

Trávníček, P., Hellinger, P., Schriver, D., 2007. Structure of Mercury's magnetosphere for different pressure of the solar wind: Three dimensional hybrid simulations. Geophys. Res. Lett. 34, doi:10.1029/2007GL029728.

Tsyganenko, N.A., 1995. Modeling the Earth's magnetospheric magnetic field confined within a realistic magnetosphere. J. Geophys. Res. 100, 5599–5612.

Zuber, M.T., Aharonson, O., Aurnou, J.M., Cheng, A.F., Hauck, S.A., Heimpel, M.H., Neumann, G.A., Peale, S.J., Phillips, R.J., Smith, D.E., Solomon, S.C., Stanley, S., 2007. The geophysics of Mercury: Current status and anticipated insights from the MESSENGER mission. Space Sci. Rev. 131, 105–132.